RSC Advances

PAPER

View Article Online
View Journal | View Issue

Cite this: *RSC Adv.*, 2020, **10**, 16972

Effects of mPEG-DSPE/corannulene or perylene nanoparticles on the ovary and oocyte†

Hongyu Wang,‡§[a] Jingwen Zhang,§[a] Daofu Feng*[b] and Xizeng Feng *[a]

Corannulene (Cor) is a polycyclic aromatic hydrocarbon (PHA) whose molecular structure is three dimensional with a unique bowl-like structure and surface charge. Perylene (Per) is similar to corannulene, with 20π electrons in its fragrance system, but it is a planar structure. Although scientists in various fields have been extensively investigating corannulene, the toxicological evaluation on organisms and its possible mechanisms remain unclear. Our objective is to investigate the toxic effects of corannulene and perylene on ovaries and oocytes. First, corannulene and perylene were wrapped with 1,2-distearoyl-*sn*-*glycero*-3-phosphoethanolamine-*N*-[methoxy(polyethyleneglycol)] (mPEG-DSPE) to form mPEG-DSPE/corannulene nanoparticles (mP-D/CoNps) and mPEG-DSPE/perylene nanoparticles (mP-D/PeNps), which enhanced their water solubility and biocompatibility. Then, the toxic effects of mP-D/CoNps or mP-D/PeNps on the quality of mouse oocytes and their possible mechanisms were studied *in vivo*. Our results indicated that mP-D/CoNps or mP-D/PeNps affected the first polar body extrusion of oocytes, increased the number of primordial follicles in the ovary, altered mitochondrial membrane potentials, induced oxidative stress and led to autophagy and apoptosis.

Received 6th March 2020
Accepted 10th April 2020

DOI: 10.1039/d0ra02129f

rsc.li/rsc-advances

1. Introduction

In recent years, with the synthesis and development of carbon nanomaterials including carbon nanotubes, graphene, fullerenes and emerging carbon nanomaterials, there has been a wave of research on the application of these diverse carbon nanomaterials in various fields. The intrinsic physicochemical properties of carbon nanomaterials make them increasingly applicable in high-performance multifunctional materials,[1–3] organic photovoltaic devices,[4,5] drug delivery and biosensors.[6] With the large-scale application of carbon nanomaterials in materials science and physical chemistry, carbon nanomaterials have certain applications in the field of biology, such as drug carriers and protective agents for cancer photothermal therapy.

Corannulene (Cor) is a polycyclic aromatic hydrocarbon (PHA), which is a three-dimensional bowl-shaped structure with surface charge consisting of a central pentagon and five closely adjacent hexagons.[7] It has a curved π surface and a large dipole moment,[8] which is a new type of carbon nanomaterial. Perylene (Per) is similar to corannulene, with 20π electrons in its fragrance system, but it has a planar structure. Importantly, corannulene and its derivatives have important applications in the field of materials science and engineering, such as a molecular switch for nanoscale machines and a motor,[9] as an important member of the organometallics,[10] for chemical encapsulation of drugs and biomolecules,[11] as a precursor for the synthesis of fullerenes[12] and an oxidation-reducing substance.[13] Moreover, perylene and its analogues have diverse applications that include fluorescence labeling[14] and fabrication of molecular electronic devices[15] and molecular sensors.

In view of the wide range of applications of carbon nanomaterials in physical chemistry and other fields, we are also interested to explore their application in biomedicine, which is premised on the evaluation of their physiological toxicity, including its harmful effects on organs such as the heart, liver, spleen, lungs and kidney, and on the nervous and reproductive systems. The toxic effects of carbon nanomaterials on organisms have been reported in many studies. For example, Makoto and his colleagues systematically summarized the results of toxicity studies of graphene-based nanomaterials in experimental animals;[16] they found that the inhalation of graphene and graphene oxides can only cause minimal lung toxicity, and large-sized graphene oxides are more toxic than the small-sized ones. Graphene-based carbon nanomaterials are mainly distributed in organs such as the lung, liver and spleen by tracheal and intravenous administration, and their distribution

[a]*College of Life Science, The Key Laboratory of Bioactive Materials, Ministry of Education, State Key Laboratory of Medicinal Chemical Biology, Nankai University, Tianjin 300071, China. E-mail: xzfeng@nankai.edu.cn*

[b]*Department of General Surgery, Tianjin Medical University General Hospital, No. 154 Anshan Road, Tianjin 300052, China. E-mail: jerryfenglc@sina.com*

† Electronic supplementary information (ESI) available. See DOI: 10.1039/d0ra02129f

‡ Current work address: Institute of Tropical Bioscience and Biotechnology, Chinese Academy of Tropical Agricultural Sciences, Haikou 571101, China.

§ These authors contributed equally to this work.

and surface characteristics lead to potential neurological, genetic and reproductive/developmental toxicity. Zhang and his colleagues studied the effects of short-term or long-term oral high-dose reductive graphene oxide nanosheets on mouse behavior.[17] The study found that high-dose reductive graphene oxide nanosheets had little effects on the exploratory behavior, anxiety and depression behaviors, and learning and memory behaviors in mice. However, exposure to reductive graphene oxides affects superoxide dismutase activity in the mouse serum, which may have effects on the motor activity, balance, and neuromuscular coordination.

Generally, carbon nanomaterial toxicity studies in organisms focus on behavioral aspects and their distribution in organs. Currently, there are relatively few studies on the effects of carbon nanomaterials on animal genetic development and reproduction. Xu and his colleagues studied the effects of long-term exposure of reductive graphene oxide nanosheets on the reproductive performance and offspring development in female mice.[18] In their study, reductive graphene oxide nanosheets were injected into the tail vein of mice at different doses and time points before or after fertilization. The sex hormone levels of adult female mice did not change significantly after injection. Female mice produced healthy offspring after the injection of reductive graphene oxide nanosheets before and during pregnancy (about 6 days). However, in the late pregnancy, low-dose or medium-dose nanosheets resulted in abortion in the mother, and most pregnant mothers died when injected with high doses of nanosheets.

Similarly, assessing the toxicity of corannulene is a prerequisite for exploring its biological applications. Research has shown that corannulene increased sleep and reduced locomotor activity and the expression of hcrt and hcrtr mRNA in zebrafish larvae.[19] Moreover, Li and his colleagues have explored the toxic effects of corannulene on mouse organs, as well as on the nervous system.[20] However, due to poor biocompatibility of corannulene and less research on its toxicity in organisms, the toxicological mechanism is still unclear, which limits its biological application. In order to enhance the water solubility and biocompatibility of corannulene and perylene,[20] they were wrapped with mPEG-DSPE (1,2-distearoyl-*sn-glycero*-3-phosphoetha-nolamine-*N*-[methoxy(polyethyleneglycol)]) to form mPEG-DSPE/corannulene nanoparticles (mP-D/CoNps) and mPEG-DSPE/perylene nanoparticles (mP-D/PeNps). To supplement the biological toxicity evaluation research on corannulene and perylene and lay a foundation for its biological function, we injected a solution containing nanoparticles into the abdominal cavity of female mice and investigated their effects on ovarian tissue, follicular development, oocyte maturation and oocyte quality.

2. Materials and methods

2.1 Reagents and animal feeding

Commercially produced perylene of 252.3093 mol g^{-1} was obtained from MERYER (M09865). Corannulene was synthesized and provided by Jay S. Siegel 8. mPEG-DSPE ($M = 2000$) was purchased from Tebu-Bio company. The chemical reagents used in this experiment, including tetrahydrofuran (THF) and physiological saline, were purchased from Tianjin Dingguo Biological Company. Pregnancy mare serum gonadotropin (PMSG), human chorionic gonadotropin (hCG) and M2 medium were purchased from Ningbo Second Hormone Factory (China).

All animal experiments were approved by the Committee on the Animal Experiments Ethics Inspection of the Nankai University and were handled in accordance with the approved guidelines. Eight-week-old female ICR mice (25–30 g body weight) were obtained from the Institute of Zoology, Chinese Academy of Sciences, and were allowed to access water and food *ad libitum*. The mice were housed under a 12 h/12 h light/darkness cycle at constant temperature (23 °C ± 2 °C).

2.2 Synthesis and characterization of mP-D/CoNps (PeNps)

Corannulene or perylene and mP-D were respectively dissolved in THF and a physiological saline solution at room temperature. Then, the corannulene or perylene/THF solution was placed in a constant-temperature water bath and heated to 78 °C. Corannulene or perylene/THF and mP-D/saline solutions were cautiously added into distilled water while continuously sonicated (1.5 s/2 s). After being signifier disrupted, the mixed solution was transferred to a water bath at 60 °C for 24 h to remove the THF solution. Corannulene or perylene and mPEG-DSPE self-assembly occurred at 60 °C. Finally, the synthesized mP-D/CoNps (PeNps) were maintained at 60 °C in a water bath. In our experiment, we used the same method as described above to treat mP-D/saline as a positive control treatment group.

Dynamic light scattering (DLS) and the absorption, emission and excitation spectra were analysed using mP-D/CoNp (PeNp) solutions diluted to 20, 25 and 40 μg mL^{-1}. Moreover, the corannulene or perylene/THF solution and mPEG-DSPE aqueous solution with concentrations of 20, 25, and 40 μg mL^{-1} were further analysed by absorption spectroscopy as the buffer and control groups, respectively.

The sample solution was dropped onto the mica slice and then dried. Afterwards, the dry sample was imaged using a Benyuan CSPM 4000 AFM (Being Nano-Instruments, Ltd). The AFM probe used was the Budget Sensors ContAI-G pobe (Innovative Solutions Bulgaria, Ltd). The particle size was measured through the height of the particles to avoid the effect of the tip convolution.[21]

2.3 mP-D/CoNp or mP-D/PeNp treatment and oocyte collection

In our experiment, mP-D/CoNps or mP-D/PeNps were dispersed in saline. Buffer-dispersed mP-D/CoNps or mP-D/PeNps (15, 30 mg kg^{-1} body weight)[13,16] were administered to mice *via* intraperitoneal injection every 24 h for 7 consecutive days. One group of control mice were administered with saline and the other group of control mice with mP-D/saline every 24 h for 7 consecutive days.

First, the mice were super-ovulated by intraperitoneal injection of 10 IU pregnant mare serum gonadotropin (PMSG). Then the mice were injected with 10 IU human chorionic

gonadotropin (hCG) after 48 h. About 14 h after the injection of hCG, the mice were killed by cervical dislocation and cumulus oocyte complexes collected from the ampulla of the oviduct were placed in an M2 medium (Ningbo second hormone factory). To obtain bare MII oocytes, we incubated the cumulus oocyte complexes with 10 mg mL^{-1} hyaluronidase for 2 min. The removed ovaries were used in western blot and qRT-PCR experiments.

2.4 Histological evaluation

After fixation with 4% paraformaldehyde at room temperature for 24 h, the tissues were dehydrated with a series of concentrations of ethanol, transparent with xylene, and finally embedded in paraffin. Paraffin-embedded ovary serial sections (5 μm) were stained with hematoxylin and eosin (HE) for light microscopic examination. Ten discontinuous sections were analyzed for each sample.

2.5 Confocal microscopy

To evaluate the intracellular mitochondrial membrane potential (MMP) and reactive oxygen species (ROS) level, at least 60 oocytes (from 3 mice in each group) were stained at 37 °C for 30 min in the darkness with 1 × JC-1 fluorochrome or 10 mM 2′,7′-dichlorodihydrofluorescein diacetate (DCFH-DA). After washing twice with PBS or 1× JC-1 wash buffer, the sample oocytes were placed on glass slides. The fluorescence images of oocytes were recorded using a confocal microscope with the same scanning settings. The fluorescence intensities were quantified using the ImageJ software.

For single staining for LC3 and Annexin-V, at least 60 oocytes (from 3 mice in each group) were fixed in 4% paraformaldehyde for 30 min and then transferred to a membrane permeabilization solution (PBS containing 0.5% Triton X-100) for 20 min at room temperature. After 1 h blocking in PBS with 1% bull serum albumin (BSA) at 4 °C, samples were incubated at room temperature for 2 h with anti-Annexin-V (1 : 200 dilution, Santa Cruz Biotechnology, USA) and anti-LC3A/B antibody (1 : 200 dilution, Cell Signaling Technology, USA). After washing three times with 1% BSA/PBS, the oocytes were labeled with specific fluorescence secondary antibodies at room temperature for 1 h. Finally, the oocytes were mounted on glass slides with an antifade mounting medium and were observed by confocal microscopy. The fluorescence intensities were quantified using the ImageJ software.

2.6 Quantitative real-time PCR

Ovary tissues were homogenized in the presence of Trizol, and total RNA was extracted from the ovary with using a TRNpure Total RNA Kit (Nobelab, Beijing, China). cDNA synthesis was performed using a PrimeScript™ RT reagent Kit with gDNA Eraser (Perfect Real Time) (Takara, China). Quantitative real-time PCR was performed with cDNAs and gene-specific primer pairs (Table S1†) mixed with a FS Universal SYBR Green PCR master mix (Roche, China) under the following conditions: 50 °C for 2 min, 95 °C for 10 min, 40 cycles of 95 °C for 15 s and 60 °C for 1 min. Data were calculated by the $2^{-\Delta\Delta C_t}$ method, and the *gapdh* mRNA levels were quantified as an endogenous control. Each sample was analyzed individually and processed in triplicate.

2.7 Western blotting

Ovary tissues from different groups were homogenized with 200 μL RIPA lysis buffer mixed with 1× protease inhibitor Cocktail (CWBiotech), and the homogenates were incubated on ice for 20 min. After centrifugation at 10 000 × *g* for 10 min, the supernatants were obtained and total tissue protein concentrations were measured by the BCA protein assay (CWBIO, China). Protein samples were mixed with a 5× SDS-PAGE sample loading buffer and boiled for 5 min. Equal amounts of protein (20 μg) were electrophoresed through 12% SDS-PAGE and then transferred onto a polyvinylidene fluoride (PVDF) membrane, which was activated in methanol for 1 min. The PVDF membranes were blocked with nonfat milk at room temperature for 2 h and then washed three times (10 min each) with Tris-buffered saline (TBS) containing 0.05% Tween-20 (TBST). The PVDF membranes were incubated with anti-Bax and anti-Bcl-2 antibodies (1 : 200 dilution, Santa Cruz Biotechnology, USA) at room temperature for 2 h and washed three times (10 min each) with TBST. The membranes were incubated with species-matched horseradish peroxidase (HRP)-conjugated secondary antibodies at room temperature for 1 h. After washing three times with TBST, the specific protein signals were visualized using an ECL Plus (Thermo Fisher Scientific). The results of western blot were quantified using the ImageJ software.

2.8 Statistical analysis

Each experiment was repeated at least three times. All data differences between control and treated mice are expressed as mean ± S.E.M. Differences were determined by Student's unpaired two-tailed *t*-test and two-way ANOVA using the GraphPad Prism software. Statistical significance was based on the *p* value: *<0.05, **<0.01, ***<0.001, and ****<0.0001.

3. Results

3.1 Characterization of mPEG-DSPE/corannulene or perylene nanoparticles

In order to enhance the water solubility of corannulene and perylene, this study encapsulated them separately with mPEG-DSPE to form mP-D/CoNps and mP-D/PeNps, as shown in Fig. 1a. First, we used an atomic force microscope (AFM) to image the synthesized mP-D/CoNps or mP-D/PeNps (Fig. 1b). To avoid the influence of the convolution particles at the tip, we measured the size of the particles by their height. The results indicated that the particle size of mP-D/CoNps and mP-D/PeNps is 100–160 nm and 110–150 nm, respectively. Fig. S1† shows the frequency distribution of nanoparticles of different sizes. Then, based on the dynamic light scattering (DLS) technology, Fig. 1c and d shows the particle size distribution of mP-D/CoNps (PeNps) in the saline buffer. Quantitative analysis results indicated that the aggregation size of mP-D/CoNps was 100–140 nm

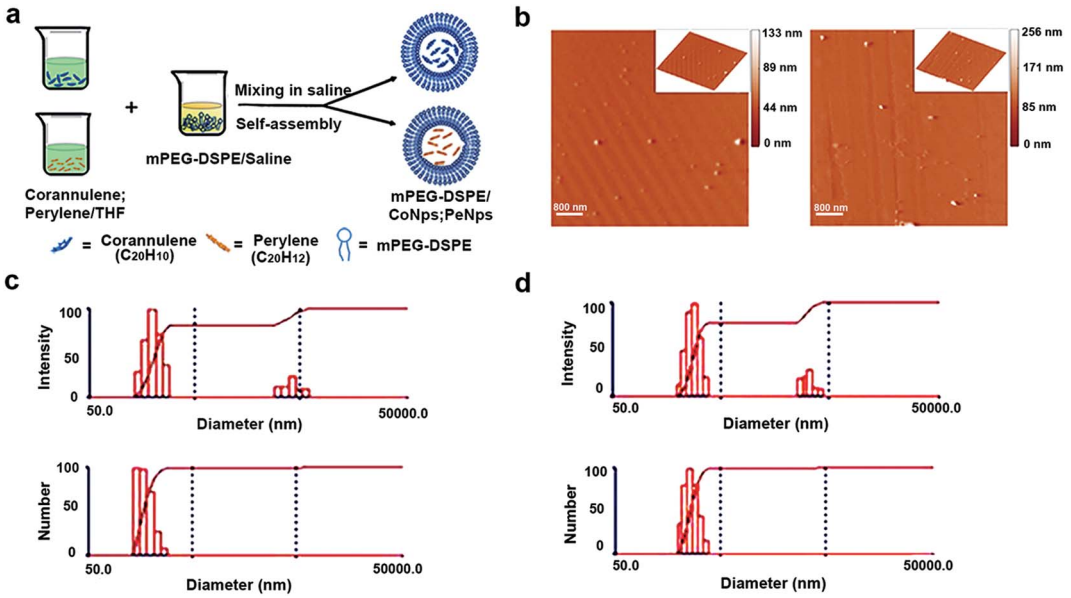

Fig. 1 Characterization of particle sizes of mP-D/CoNps or mP-D/PeNps. (a) Schematic of the synthesis of mP-D/CoNps or mP-D/PeNps. (b) Atomic force microscopic images of mP-D/CoNps and mP-D/PeNps; (c) average particle size distribution (number and intensity of particles) of mP-D/CoNps. (d) Average particle size distribution (number and intensity of particles) of mP-D/PeNps.

and mP-D/PeNps was 110–140 nm in the saline buffer. In addition, only a small number of particles aggregated, and the size is in the range of 200–275 nm.

3.2 mP-D/CoNp or mP-D/PeNp treatment reduced PBE rates and increased ROS levels

The process of oocytes from recovering meiosis to the stage of MII is usually called oocyte maturation, so we measured the percentage of PBE in oocytes isolated from mice administered with mP-D/CoNps or mP-D/PeNps (15 and 30 mg kg^{-1}) *via* intraperitoneal injection for 7 consecutive days. In Fig. 2a and b, the results indicated that D/PeNp (61.53 ± 0.87, $p < 0.05$) treatment reduced the PBE rate compared to the control group (67.20 ± 1.13). There was no significant difference in the treatment with low doses (mP-D/CoNps: 64.65 ± 1.372; mP-D/PeNps: 64.41 ± 0.92). Thus, high doses were used in the subsequent study.

Oxidative stress is a cellular response to noxious external stimuli. To determine whether mP-D/CoNps or mP-D/PeNps induced oxidative stress in mice, we first evaluated the ROS levels in MII oocytes. As shown in Fig. 2c, most of the control and mP-D group MII oocytes showed low fluorescence intensity, indicating low ROS production. In Fig. 2d, ROS fluorescence intensities were elevated for the experimental groups treated with mP-D/CoNps (14.88 ± 0.1862, $p < 0.0001$) and mP-D/PeNps (44.73 ± 0.2161, $p < 0.0001$) compared to the control (8.264 ± 0.1395) and mP-D (7.853 ± 0.1485) groups. Then, we examined the oxidative stress–related genes by qRT-PCR. Fig. 2e shows that *cat* mRNA expression levels increased in oocytes obtained from mP-D/CoNp (5.89 ± 1.03, $p < 0.0001$) or mP-D/PeNp (4.46 ± 0.22, $p < 0.0001$) groups as compared to those obtained from the control group (1.01 ± 0.09). *gpx* mRNA expression levels increased in oocytes obtained from mP-D/CoNps (3.47 ± 0.20, $p < 0.01$) or mP-D/PeNp (6.99 ± 0.19, $p < 0.0001$) groups as compared to those obtained from the control group (1.01 ± 0.11). In addition, *sod2* mRNA expression levels significantly increased in oocytes from mP-D/PeNp groups (3.40 ± 0.47, $p < 0.0001$) as compared to those from the control group (1.01 ± 0.09). However, there was no significant difference in mRNA levels between the control and mP-D groups.

3.3 mP-D/CoNp or mP-D/PeNp treatment affected the mitochondrial function

Mitochondria function is related to the production of ROS and can be used as an important indicator to measure the quality of oocytes. Furthermore, we explored whether mP-D/CoNps (PeNps) can adversely affect the oocyte mitochondrial function. We stained oocytes with JC-1 dye to measure the mitochondrial membrane potential. The oocytes of the control group and the mP-D group showed strong red fluorescence, indicating that they had high mitochondrial membrane potential (control: 1.01 ± 0.08; mP-D: 0.95 ± 0.09). Compared with the control group, mP-D/CoNp (PeNp) treatment reduced the mitochondrial membrane potential of the oocyte (Fig. 3a). A lower ratio of the red/green fluorescence intensity represented mitochondrial injury. As shown in Fig. 3b, quantitative analysis showed a significant decrease in the ratio of red to green JC-1 fluorescence after mP-D/CoNp (0.43 ± 0.01, $p < 0.001$) and mP-D/PeNp (0.40 ± 0.01, $p < 0.001$) treatment.

3.4 mP-D/CoNp or mP-D/PeNp treatment resulted in early apoptosis

The decrease in mitochondrial membrane potential is a landmark event in the early stages of apoptosis. Next, we assessed

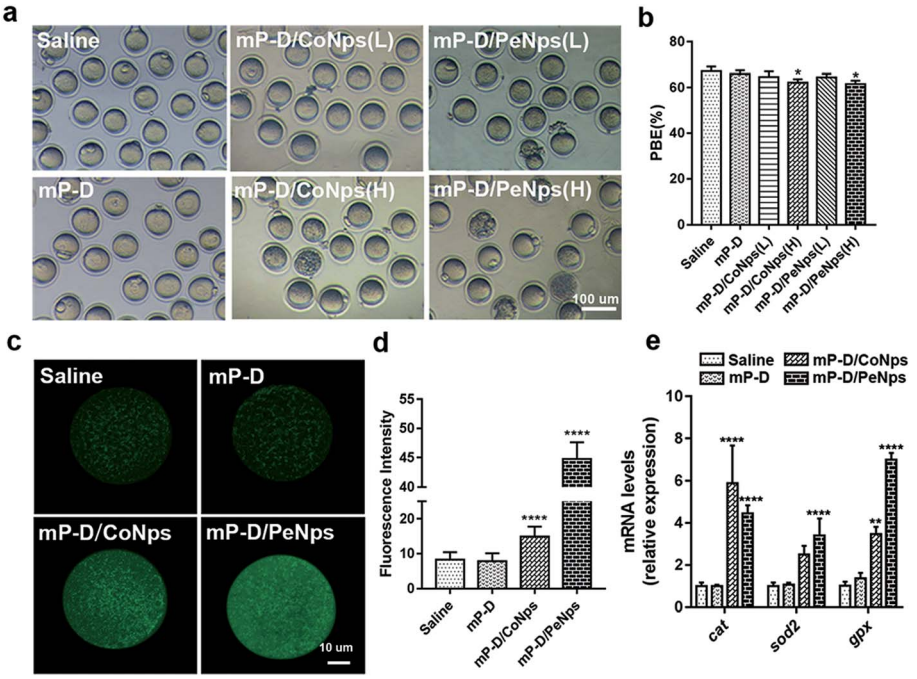

Fig. 2 mP-D/CoNp or mP-D/PeNp treatment reduced the PBE rate and increased the ROS levels. (a) Representative images of MII stage oocytes from different groups of mice. (b) Effect of different treatments on the PBE rate *in vivo*. (c) Representative images of ROS levels in oocytes. (d) Fluorescence intensities of ROS in oocytes were analysed using ImageJ. (e) Expressions of oxidative stress-related genes in MII stage oocytes. Data were analyzed by the unpaired *t*-test and two-way ANOVA test. Data are expressed as mean ± S.E.M. * represents the significant difference compared with the saline group. *$p < 0.05$, **$p < 0.01$, ****$p < 0.0001$.

early apoptosis by staining oocytes with an Annexin V-FITC antibody. The results indicated that the green fluorescence signals were much stronger in oocytes from the mP-D/CoNp or mP-D/PeNp groups as compared to those in control and mP-D groups (Fig. 4a). In Fig. 4b, the rate of apoptotic oocytes was dramatically higher in the mP-D/CoNp (78.67 ± 1.76, $p < 0.0001$) or mP-D/PeNp groups (78.67 ± 1.76, $p < 0.0001$) than that in control (14.33 ± 0.88) and mP-D (16.58 ± 0.62) groups. In Fig. 4c, qRT-PCR results showed that *caspase-3* and *bax* mRNA expression levels were significantly increased in the mP-D/CoNps (*caspase-3*: 2.76 ± 0.16, bax: 3.17 ± 0.56, $p < 0.01$) or mP-D/PeNps groups (*caspase-3*: 3.16 ± 0.27, $p < 0.01$, *bax*: 4.14 ± 0.49, $p < 0.001$) compared the control (*caspase-3*: 1.01 ± 0.10, *bax*: 1.00 ± 0.06) and mP-D groups (*caspase-3*: 1.54 ± 0.31, *bax*: 1.47 ± 0.04). Additionally, we further evaluated whether different treatments influenced the expression levels of

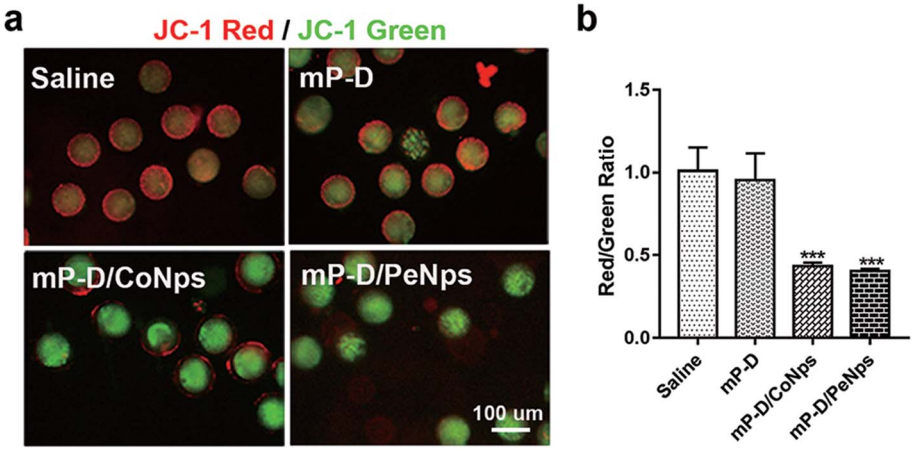

Fig. 3 mP-D/CoNp or mP-D/PeNp treatment has effects on the mitochondrial function. (a) Fluorescence photographs of mitochondrial function detected by JC-1 in four groups. (b) Comparison of the relative ratios of red/green fluorescence intensities stained by JC-1 in four groups. Data were analyzed by the unpaired *t*-test. Data are expressed as mean ± S.E.M. * represents the significant difference compared with the saline group. ***$p < 0.001$.

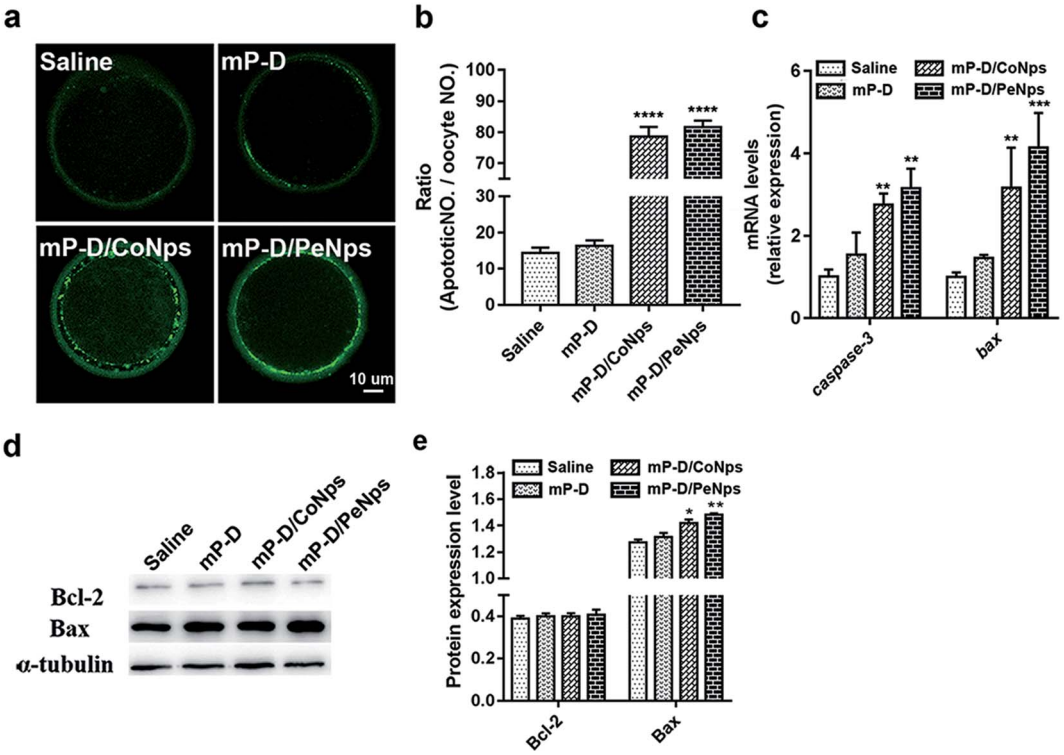

Fig. 4 mP-D/CoNps or PeNps treatment resulted in early apoptosis. (a) Representative images of apoptotic oocytes from groups. (b) The rate of early apoptosis was recorded in four groups. (c) Expressions of apoptosis-related genes in oocytes. (d) Western blot analyses protein expression of Bcl-2 and Bax. (e) Relative Bcl-2 and Bax bands intensity were assessed by ImageJ software. Data are analyzed by unpaired *t*-test and two-way ANOVA test. Data are expressed as mean ± S.E.M. * represents significantly different compared with the saline group. $*p < 0.05$, $**p < 0.01$, $***p < 0.001$, $****p < 0.0001$.

apoptotic proteins. In Fig. 4d and e, western blot results showed that Bcl-2 protein expressions between groups showed no significant difference (saline: 0.39 ± 0.01; mP-D: 0.40 ± 0.01; mP-D/CoNps: 0.40 ± 0.01; mP-D/PeNps: 0.41 ± 0.01), and Bax protein expressions were increased compared with the control (1.28 ± 0.01) and mP-D (1.31 ± 0.02) groups after treatment with mP-D/CoNps (1.42 ± 0.01, $p < 0.05$) or mP-D/PeNps (1.48 ± 0.01, $p < 0.01$). Collectively, our results indicated that mP-D/CoNp or mP-D/PeNp treatment induced early apoptosis in oocytes.

3.5 mP-D/CoNp or mP-D/PeNp treatment resulted in autophagy

Apoptosis and autophagy are essential basic physiological mechanisms for maintaining cell and body homeostasis. Therefore, we also assessed autophagy level in oocytes by immunofluorescence staining of LC3, which is a membrane constituent of functional autophagosomes. As shown in Fig. 5a and b, oocytes from mP-D/CoNp (14.5 ± 0.39, $p < 0.0001$) or mP-D/PeNp (15.57 ± 0.35, $p < 0.0001$) groups had a stronger fluorescence intensity than those from the control (6.56 ± 0.14) and mP-D (8.07 ± 0.16) groups. In Fig. 5c, qRT-PCR results indicated that *lc3*, *atg14* and *beclin1* mRNA expression levels were significantly increased in the mP-D/CoNp (*lc3*: 2.43 ± 0.51, *atg14*: 2.67 ± 0.34, $p < 0.01$, *beclin1*: 4.76 ± 0.27, $p < 0.0001$) or mP-D/PeNp (*lc3*: 2.43 ± 0.51, *atg14*: 2.67 ± 0.34, $p < 0.01$, *beclin1*: 10.37 ± 0.28, $p < 0.0001$) groups compared with that of the control (*lc3*: 1.00 ± 0.05, *atg14*: 1.00 ± 0.04, *beclin1*: 1.00 ± 0.04) and mP-D (*lc3*: 1.41 ± 0.36, *atg*14: 1 ± 0.04, *beclin1*: 1.07 ± 0.12) groups. Our results indicated that mP-D/CoNp or mP-D/PeNp treatment induced autophagy in oocytes.

3.6 mP-D/CoNp or mP-D/PeNp treatment hindered follicular development

To investigate how mP-D/CoNps or mP-D/PeNps disrupted oogenesis, we carefully analyzed follicle development in different groups. After 7 days of treatment, the ovaries were taken out for histological examination. Representative HE histological slices of ovaries of the control and experimental groups were analysed (Fig. 6a). We found that the percentage of primordial follicles, determined by the analysis of histological sections, was drastically increased in the group treated with mP-D/CoNps or mP-D/PeNps, as shown in Fig. 6b (control: 15.80 ± 0.44%; mP-D: 14.92 ± 1.67%; mP-D/CoNps: 30.05 ± 1.00%, $p < 0.001$; mP-D/PeNps: 31.86 ± 1.93%, $p < 0.001$). In Fig. 6c and d, the percentage of primary follicles and secondary follicles was observably reduced in mP-D/CoNps or mP-D/PeNp groups (primary follicles: control: 27.43 ± 1.19%; mP-D: 24.00 ± 0.74%; mP-D/CoNps: 12.24 ± 1.13%, $p < 0.0001$; mP-D/PeNps: 14.52 ± 0.41%, $p < 0.0001$; secondary follicles: control: 30.37 ± 0.90%; mP-D: 31.96 ± 1.65%; mP-D/CoNps: 15.80 ± 1.29%, $p < 0.0001$;

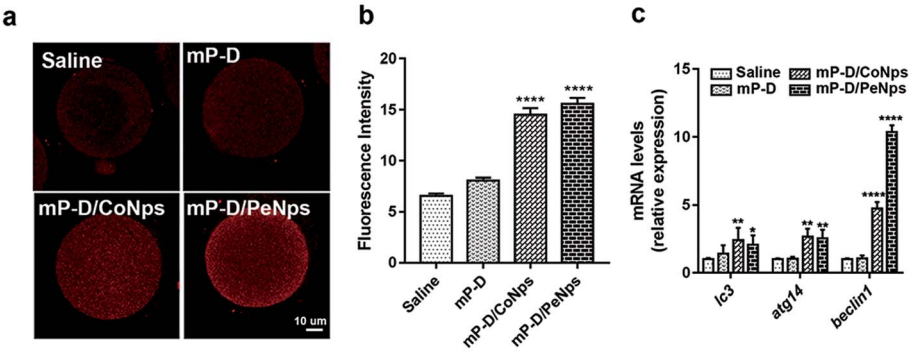

Fig. 5 mP-D/CoNp or mP-D/PeNp treatment resulted in early autophagy. (a) Representative confocal images of autophagosome (LC3 puncta) distribution in oocytes from groups. (b) Fluorescence intensities of LC3 in oocytes were analysed using ImageJ. (c) Expressions of autophagy-related genes in oocytes. Data were analyzed by the unpaired *t*-test and two-way ANOVA test. Data are expressed as mean ± S.E.M. * represents the significant difference compared with the saline group. $^{**}p < 0.01$, $^{****}p < 0.0001$.

mP-D/PeNps: 12.84 ± 0.51%, $p < 0.0001$). In Fig. 6e, there was no significant difference in the percentage of atresia follicles between the control and experimental groups (control: 23.06 ± 0.96%; mP-D: 24.15 ± 0.10%; mP-D/CoNps: 23.99 ± 1.21%; mP-D/PeNps: 24.503 ± 1.81%).

4. Discussion

Carbon nanomaterials have many applications in materials science and other fields, and the research of the toxicity of carbon nanomaterials has been widely concerned. In recent years, there have been many studies on neurotoxicity and visceral toxicity of carbon nanomaterials[16] containing carbon nanotubes, graphene oxides and carbon black, so we speculate that carbon nanomaterials may also affect the reproductive ability of female mice, but there are few studies on toxicity in this field. In this study, we considered that mP-D/CoNps or mP-D/PeNps could contribute to the destruction of oocyte development. Then, the toxicity of mP-D/CoNps or mP-D/PeNps and its underlying mechanisms were explored including oocyte

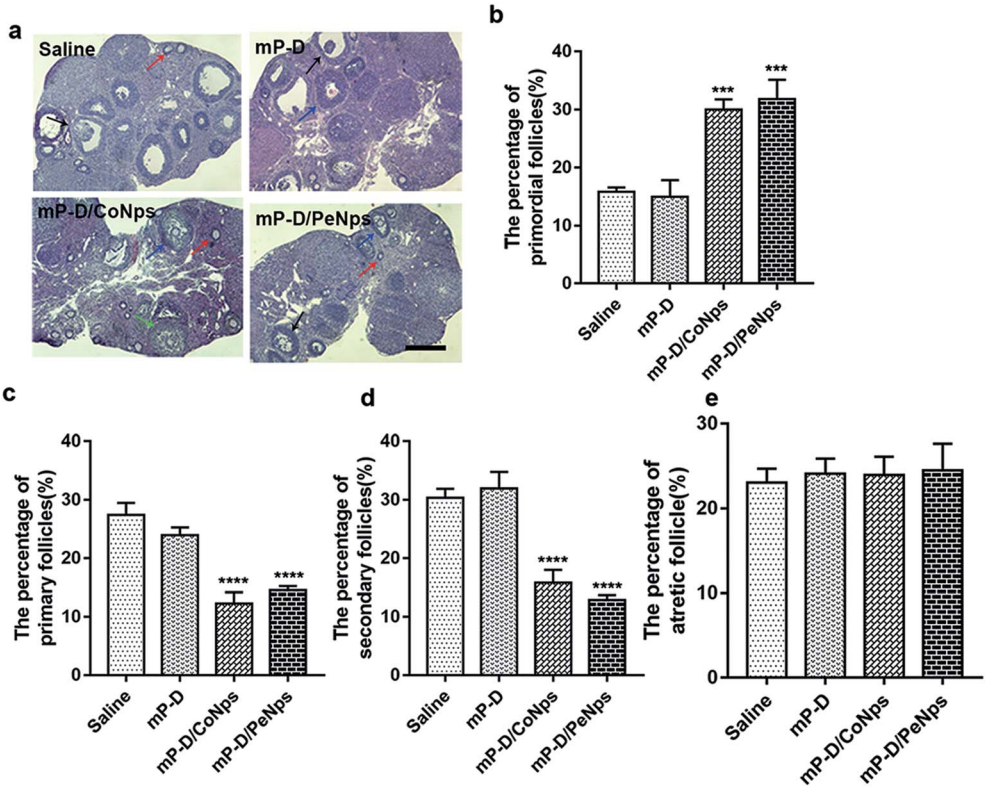

Fig. 6 The effects of mP-D/CoNps or PeNps treatment on ovaries. (a) Representative images of HE stained of ovaries from the four group. Scale bar indicates 100 μm. Red arrow: Primordial follicles; blue arrow: primary follicles; black arrow: secondary follicles; green arrow: atresia follicles. (b–e) The ratio of the follicles at different periods of oocytes in four groups. Data are analyzed by unpaired *t*-test. Data are expressed as mean ± S.E.M. * represents significantly different compared with the saline group. $^{***}p < 0.001$, $^{****}p < 0.0001$.

polar body extrusion, oxidative stress, mitochondrial membrane potential, autophagy and apoptosis (Fig. 7).

To confirm our hypothesis, we examined the oocyte meiotic progression by the extrusion of the first polar body and the crucial events of the high-quality oocyte in female reproduction.[22] We found that the polar rate of oocytes decreased in the experimental group (Fig. 2). The decreased PBE rate indicated that the mP-D/CoNps or mP-D/PeNps may be activated to arrest the oocyte at the MI stage. The basic functional unit of oocyte generation and development is follicles, and increased atresia follicles can adversely affect the quality of oocytes.[23–26] Then, we performed histological examination of the ovary by hematoxylin-eosin staining (Fig. 6). The results indicated that the total number of follicles in mP-D/CoNp or mP-D/PeNp groups decreased and the development of follicles was delayed, so that most of the follicles were in the primordial follicle phase, while the number of primary and secondary follicles decreased significantly. There was no significant difference in mP-D/CoNp or mP-D/PeNp groups compared with the control, with reference to the percentage of atretic follicles. These results indicated that mP-D/CoNps or mP-D/PeNps had a negative effect on oocyte maturation.

Under physiological conditions, ROS and antioxidants are maintained at a balanced level. ROS are produced by the metabolism of surrounding oocytes,[27] which is responsible for the poor quality of oocytes.[28] An increase in the ROS levels causes oxidative damage stimulated by foreign substances such as chemical poisons and exposure to light and radiations.[29–31] Then, we examined the oxidative stress level, and found that the ROS levels increased. During the maturation of oocytes, the increase in ROS levels is mainly due to physiological metabolism and the mechanism of antioxidant enzymes in the body.[29,32] The antioxidant enzyme system in the body mainly includes superoxide dismutase (SOD), catalase (CAT) and glutathione peroxidase (GPX).[33] SOD is a natural superoxide free radical scavenging factor in the body, which can convert the harmful superoxide free radical into hydrogen peroxide (H_2O_2). Although H_2O_2 is still a harmful reactive oxygen species, CAT in the body immediately breaks it down into perfectly harmless water and oxygen, while GPX also clears it out. Our results indicated that the mRNA levels of *cat*, *sod* and *gpx* obviously increased after mP-D/CoNp or mP-D/PeNp treatment. Since the expression levels of *sod* and *gpx* in the mP-D/PeNP group were significantly higher than those in the mP-D/CoNP group, it was found that mP-D/PeNPs might have resulted in higher rates of ROS generation.[34]

Mitochondria are the most sensitive part of ROS and the main organelles that provide energy in oocytes, whose activity is closely related to the quality of oocytes.[35] The level of metabolism of mitochondria determines whether all functional activities of cells can be effectively carried out. Membrane potential is one of the important markers of mitochondrial activity.[36] The level of mitochondrial membrane potential can partially reflect the metabolic state and developmental potential of oocytes.[25,37–40] This study shows that the mitochondrial membrane potential of oocytes decreased in mP-D/CoNp or mP-D/PeNp groups. After mP-D/CoNp or mP-D/PeNp treatment, the mitochondria of mouse oocytes were damaged.

Decreased mitochondrial membrane potential is a hallmark of early cell apoptosis.[41] Our results indicated that ROS production is induced in mouse oocytes exposed to the mP-D/CoNps or mP-D/PeNps and the expression of oxidative stress-related genes is increased. Excessive production of ROS can regulate cell growth and development in a multi-interaction relationship.[42,43] Therefore, we then detected apoptosis and autophagy. The results obtained in our study indicated that the rate of apoptosis of oocytes was dramatically higher in the mP-D/CoNp or mP-D/PeNp groups. Apoptosis was induced when the pro-apoptotic protein Bax formed homologous dimers. When Bax and apoptotic protein Bcl-2 form heterodimers, apoptosis is inhibited.[44] After receiving the apoptotic signal, the molecular conformation of Bax changes, translocates and inserts into the mitochondrial outer membrane, which destroys the integrity of the mitochondrial membrane. The mitochondria release apoptotic factors such as cytochrome-c, and initiate the caspase cascade reaction to activate *caspase-3*. Our results indicated that although there was no significant difference in the expression of Bcl-2 in all groups, the expression of Bax and *caspase-3*

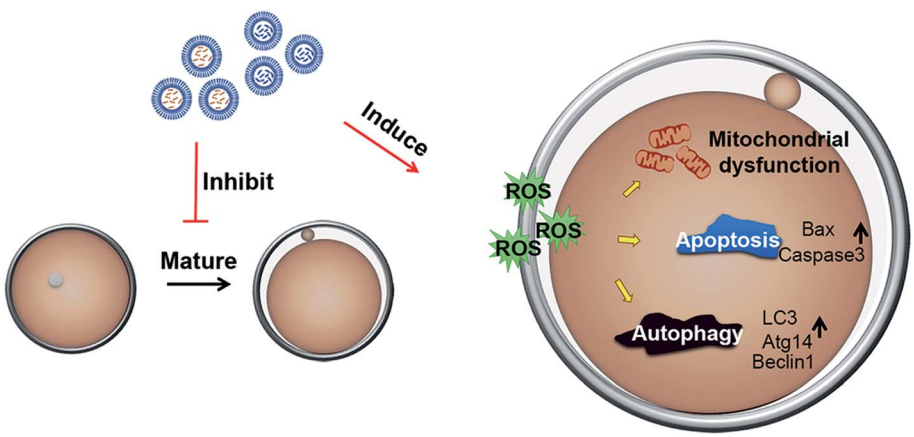

Fig. 7 Potential mechanism of mP-D/CoNp- or mP-D/PeNp-induced cytotoxicity in mouse oocytes.

increased in the treatment groups. The expression levels of apoptosis-related proteins and genes are consistent with the early apoptotic state of oocytes.[42] Meanwhile, our results indicated that mouse oocytes treated with mP-D/CoNps or mP-D/PeNps also exhibited autophagy. In the initiation stage of autophagosome formation, autophagy-related protein 7 (ATG7) activates light chain 3 (LC3) and facilitates the formation of the ATG12–ATG5–ATG16L1 complex.[45] Beclin-1 is also integral to the vesicle nucleation phase of autophagosome formation in mammals.[46] qRT-PCR results indicated that *lc3*, *atg14* and *beclin1* mRNA expression levels were significantly increased in the treatment groups.

5. Conclusion

In summary, female mice were injected intraperitoneally with mP-D/corannulene (perylene) nanoparticles to investigate their toxicity in this study. The results indicated that the nanoparticles had little effects on follicle production and polar body extrusion (PBE) rate in female mice, but they increased the ROS level in oocytes, which led to decreased mitochondrial function in the oocytes, triggering apoptosis and autophagy. Our research provided the potential mechanism of mP-D/CoNp or mP-D/PeNp toxicity in oocytes.

Funding sources

This work was supported by the Special Fund for Basic Research on Scientific Instruments of the Chinese National Natural Science Foundation [Grant no. U1613220, and 61633012], and the National Basic Research Program (973 program) of China [Grant no. 2015CB856500].

Conflicts of interest

There are no conflicts to declare.

Acknowledgements

This project was initiated in the College of Life Science, The Key Laboratory of Bioactive Materials, Ministry of Education of Nankai University.

References

1 Y. Liu and B. Yan, *ACS Appl. Mater. Interfaces*, 2017, **9**, 18626–18638.
2 Y. Zhang, T. Zou, M. Guan, M. Zhen, D. Chen, X. Guan, H. Han, C. Wang and C. Shu, *ACS Appl. Mater. Interfaces*, 2016, **8**, 11246–11254.
3 R. H. Tunuguntla, R. Y. Henley, Y. C. Yao, T. A. Pham, M. Wanunu and A. Noy, *Science*, 2017, **357**, 792–796.
4 D. M. Guldi and M. Prato, *Acc. Chem. Res.*, 2000, **33**, 695–703.
5 Y. L. Wu, M. C. Stuparu, C. Boudon, J. P. Gisselbrecht, W. B. Schweizer, K. K. Baldridge, J. S. Siegel and F. Diederich, *J. Org. Chem.*, 2012, **77**, 11014–11026.
6 F. De Leo, A. Magistrato and D. Bonifazi, *Chem. Soc. Rev.*, 2015, **44**, 6916–6953.
7 D. Pappo, T. Mejuch, O. Reany, E. Solel, M. Gurram and E. Keinan, *Org. Lett.*, 2009, **11**, 1063–1066.
8 M. Juricek, N. L. Strutt, J. C. Barnes, A. M. Butterfield, E. J. Dale, K. K. Baldridge, J. F. Stoddart and J. S. Siegel, *Nat. Chem.*, 2014, **6**, 222–228.
9 B. L. Feringa, *Angew. Chem., Int. Ed.*, 2017, **56**, 11060–11078.
10 A. S. Filatov, A. Y. Rogachev, E. A. Jackson, L. T. Scott and M. A. Petrukhina, *Organometallics*, 2010, **29**, 1231–1237.
11 A. Sygula and S. Saebø, *Int. J. Quantum Chem.*, 2009, **109**, 65–72.
12 L. T. Scott, *Angew. Chem., Int. Ed.*, 2004, **43**, 4994–5007.
13 B. Gholamine, I. Karimi, A. Salimi, P. Mazdarani and L. A. Becker, *Toxicol. Ind. Health*, 2017, **33**, 340–350.
14 C. Julien, A. Debarre, D. Nutarelli, A. Richard and P. Tchenio, *J. Phys. Chem. B*, 2005, **109**, 23145–23153.
15 C. Flors, I. Oesterling, T. Schnitzler, E. Fron, G. Schweitzer, M. Sliwa, A. Herrmann, M. vanderAuweraer, F. C. deSchryver and K. Mullen, *J. Phys. Chem. C*, 2007, **111**, 4861–4870.
16 M. Ema, M. Gamo and K. Honda, *Regul. Toxicol. Pharmacol.*, 2017, **85**, 7–24.
17 D. Zhang, Z. Zhang, Y. Liu, M. Chu, C. Yang, W. Li, Y. Shao, Y. Yue and R. Xu, *Biomaterials*, 2015, **68**, 100–113.
18 S. Xu, Z. Zhang and M. Chu, *Biomaterials*, 2015, **54**, 188–200.
19 X. Li, Y. Zhang, X. Li, D. Feng, S. Zhang, X. Zhao, D. Chen, Z. Zhang and X. Feng, *Acta Biomater.*, 2017, **55**, 271–282.
20 X. Li, D. Sun, X. Li, D. Zhu, Z. Jia, J. Jiao, K. Wang and D. Kong, *Biomater. Sci.*, 2017, **5**, 849–859.
21 J. Canet-Ferrer, E. Coronado, A. Forment-Aliaga and E. Pinilla-Cienfuegos, *Nanotechnology*, 2014, **25**, 395703.
22 M. Zhang, Y. Miao, Q. Chen, M. Cai, W. Dong, X. Dai, Y. Lu, C. Zhou, Z. Cui and B. Xiong, *FASEB J.*, 2018, **32**, 342–352.
23 V. Rossi, M. Lispi, S. Longobardi, M. Mattei, F. D. Rella, A. Salustri, M. D. Felici and F. G. Klinger, *Cell Death Differ.*, 2017, **24**, 72–82.
24 S. Yin and X. Jiang, *Development*, 2017, **144**, 2165–2174.
25 Y. Liu, Y. L. Wang, S. W. He, M. H. Chen, Z. Zhang, X. P. Fu, B. B. Fu, B. Q. Liao, Y. H. Lin, Z. Q. Qi and H. L. Wang, *Oncotarget*, 2017, **8**, 6233–6245.
26 M. Wu, L. Ma, L. Xue, W. Ye, Z. Lu, X. Li, Y. Jin, X. Qin, D. Chen, W. Tang, Y. Chen, Z. Hong, J. Zhang, A. Luo and S. Wang, *Aging*, 2019, **11**, 1030–1044.
27 N. Sugino, *Reprod. Med. Biol.*, 2005, **4**, 31–44.
28 H. Tamura, A. Takasaki, I. Miwa, K. Taniguchi, R. Maekawa, H. Asada, T. Taketani, A. Matsuoka, Y. Yamagata, K. Shimamura, H. Morioka, H. Ishikawa, R. J. Reiter and N. Sugino, *J. Pineal Res.*, 2008, **44**, 280–287.
29 S. I. Zandalinas and R. Mittler, *Free Radical Biol. Med.*, 2018, **122**, 21–27.
30 Y. Jiang, X. Yu, C. Su, L. Zhao and Y. Shi, *Artif. Cells, Nanomed., Biotechnol.*, 2019, **47**, 747–756.
31 D. Hui, L. Yun, J. Wang, Y. Nie, Y. Sun, M. Wang, D. Wang, Y. Zhen, C. Lei and J. Wang, *Environ. Sci.: Nano*, 2018, **5**, 1711–1728.

32 L. He, T. He, S. Farrar, L. Ji, T. Liu and X. Ma, *Cell. Physiol. Biochem.*, 2017, **44**, 532–553.
33 X. Cheng, D. X. Gao, J. J. Song, F. Z. Ren and X. Y. Mao, *RSC Adv.*, 2015, **5**, 4511–4523.
34 Y. Li, Z. Zhang, C. He, K. Zhu, Z. Xu, T. Ma, J. Tao and G. Liu, *J. Pineal Res.*, 2015, **59**, 365–375.
35 Q. Chen, E. J. Vazquez, S. Moghaddas, C. L. Hoppel and E. J. Lesnefsky, *J. Biol. Chem.*, 2003, **278**, 36027–36031.
36 U. Gautam, R. Srinivasan, A. Rajwanshi, D. Bansal and R. K. Marwaha, *Cancer*, 2008, **114**, 494–503.
37 S. Liang, M. H. Zhao, S. A. Ock, N. H. Kim and X. S. Cui, *Environ. Toxicol.*, 2016, **31**, 1486–1495.
38 L. Zhang, X. Xue, J. Yan, L. Y. Yan, X. H. Jin, X. H. Zhu, Z. Z. He, J. Liu, R. Li and J. Qiao, *Sci. Rep.*, 2016, **6**, 26326.
39 L. Zhang, Z. Zhang, J. Wang, D. Lv, T. Zhu, F. Wang, X. Tian, Y. Yao, P. Ji and G. Liu, *J. Pineal Res.*, 2019, **66**, e12550.
40 Y. Liu, Y. L. Wang, M. H. Chen, Z. Zhang, B. H. Xu, R. Liu, L. Xu, S. W. He, F. P. Li, Z. Q. Qi and H. L. Wang, *Mol. Reprod. Dev.*, 2016, **83**, 768–779.
41 M. Reers, T. W. Smith and L. B. Chen, *Biochemistry*, 1991, **30**, 4480–4486.
42 Z. Z. Jia, J. W. Zhang, D. Zhou, D. Q. Xu and X. Z. Feng, *Chemosphere*, 2019, **223**, 704–713.
43 M. E. Pepling, *Reproduction*, 2012, **143**, 139–149.
44 L. Lalier, P.-F. o Cartron, P. Juin, S. Nedelkina, S. Manon, B. Bechinger and F. o M Vallette, *Apoptosis*, 2007, **12**, 887–896.
45 N. Mizushima and M. Komatsu, *Cell*, 2011, **147**, 728–741.
46 T. Zhihan, M. Xinyi, L. Qingying, G. Rufei, Z. Yan and C. Xuemei, *J. Cell. Physiol.*, 2019, **234**, 6125–6135.